Journal of Environmental Science and Technology

ISSN 1994-7887

science alert

ANSInet
an open access publisher
http://ansinet.com

OPEN ACCESS Journal of Environmental Science and Technology

ISSN 1994-7887
DOI: 10.3923/jest.2019.65.80

Research Article
Brilliant Green Dye Sorption onto Snail Shell-rice Husk: Statistical and Error Function Models as Parametric Isotherm Predictors

Lekan Taofeek Popoola, Adeyinka Sikiru Yusuff, Olusola Adedayo Adesina and Mayowa Adeoye Lala

Unit Operation and Material Science Laboratory, Department of Chemical and Petroleum Engineering , Afe Babalola University, Ado-Ekiti, Ekiti State, Nigeria

Abstract

Background and Objective: Incessant increase in the pollution of water bodies due to brilliant green dye (BGD) discharge from forms of industrial activities has called for its adsorption isotherm parameter prediction for efficient design of equipment for BGD uptake from aqueous solution. In this study, a low-cost composite adsorbent was prepared from snail shell and rice husk (SS-RH) via calcination for brilliant green dye (BGD) adsorption from aqueous solution. **Materials and Methods:** Six two-parameter and three three-parameter isotherm models were used to fit the experimental data by both linear and non-linear regression methods using 10 error functions. The SEM, FTIR and EDS were used to characterize the adsorbent. **Results:** Langmuir and Sip were the most fitted isotherm models for the process. Chi-square (χ^2) predicted well for two-parameter isotherm study while EABS, HYBRID and NSD predicted well for non-linear R-P, Sips and Toth models, respectively. The SEM revealed irregular surface texture for the SS-RH with pore openings filled with BGD. The FTIR revealed shift in spectrum broad peaks after adsorption. Active mixed metal oxides were formed with change in weight percentage after adsorption by EDS. **Conclusion:** Predicted isotherm parameters proved applicable for effective adsorption column design. Statistical error functions were efficient to tackle discrepancies of data arising from measurement error. Also, snail shell-rice husk adsorption capacity and surface properties proved it as effective adsorbent for brilliant green dye removal from aqueous solution.

Key words: Snail shell-rice husk, brilliant green dye, linear regression, non-linear regression, error functions

Citation: Lekan Taofeek Popoola, Adeyinka Sikiru Yusuff, Olusola Adedayo Adesina and Mayowa Adeoye Lala, 2019. Brilliant green dye sorption onto snail shell-rice husk: Statistical and error function models as parametric isotherm predictors. J. Environ. Sci. Technol., 12: 65-80.

Corresponding Author: Lekan Taofeek Popoola, Unit Operation and Material Science Laboratory, Department of Chemical and Petroleum Engineering, Afe Babalola University, Ado-Ekiti, Ekiti State, Nigeria Tel: +2348062397669

Competing Interest: The authors have declared that no competing interest exists.

Data Availability: All relevant data are within the paper and its supporting information files.

INTRODUCTION

In recent times, ecosystems have been worsened due to adverse effects from neo-industrial activities causing great threat to human health and the environment in which he lives. Among these is the continuous rise in the pollution of water bodies resulting from discharge of brilliant green dye from textile, printing, pharmaceutical, pulp and paper, carpet, kraft bleaching and tannery industries[1] being assisted by the exponential rise in the world population[2]. Brilliant green dye (BGD) is a synthesized cationic dye with mutagenic, carcinogenic and toxic attributes causing havoc to different microbiological species[3]. Thus, a proficient technique is required in the removal of BGD pollutants from water bodies as it is estimated that about 30% of dye used remains unfixed[4] due to their high stability and resistance to biodegradation[5]. A broad range of methods such as electrochemical technique[6], nanofiltration membranes[7], advanced oxidation and microfiltration[8], ultrasonic technique[9], photocatalytic degradation[10], coagulation[11], membrane separation[12], merged photo-Fenton and biological oxidation[13], ozonation[14], bioremediation[15], aerobic degradation[16], photo-degradation[17] and adsorption[18] have been proposed in treatment of waste water contaminated with dyes. However, their respective advantages and shortcomings had been presented in literatures[19-24] with adsorption being considered as an outstanding method of contaminated waste water treatment[25,26] due to its simplicity, availability, low cost, technically viable, high performance and socially satisfactory features[27,28]. Numerous adsorbents synthesized from low-cost natural materials such as wheat shell[29], eggshell[30], saw dust[31], clay[32], bamboo charcoal[33], guava leaf powder[34], pinang frond[35] and so on had been used for the removal of coloured dyes from aqueous solution.

In general, information obtained from simulation results of equilibrium isotherms of adsorption using experimental data is very imperative. Adsorption isotherms explained pollutants interaction with the used adsorbent at constant temperature. Parameters obtained from this are very crucial as they are applicable for (1) Adsorption mechanism pathways optimization (2) Adsorption systems effective design purposes and (3) Surface properties and adsorbents capacities expression[36,37]. To achieve these, the use of error analyses is required for accurate and consistent adsorption parameters prediction to enable adequate adsorption equilibrium correlations establishment[38]. Nevertheless, data obtained from series of batch adsorption experiments have discrepancies resulting from measurement error which in return affect data accuracy. Thus, statistical error functions are effective tools to tackle great challenges of data errors to affirm accurate measurement results and better fitness of equation to experimental data.

Though rice husk and coconut shell had been used separately for adsorption of methylene blue from aqueous solution[39], a novel low-cost composite adsorbent prepared from snail shell and rice husk (SS-RH) was used for the adsorption of brilliant green dye (BGD) from aqueous solution in this study. Two-parameters (Freundlich, Langmuir, Temkin, Dubinin-Radushkevich, Harkin-Jura and Halsey) and three-parameters (Redlich-Peterson, Sips and Toth) isotherm models were used to fit the experimental data. Because of the main shortcomings of linear regression method in fitting model and its parameters evaluation which include: (1) Error changes discrepancy[40] and (2) Unsuitability for models with more than two parameters[41], both linear and non-linear regression methods were used to test the fitness of these models and their parameters evaluation using non-linear chi-square test (χ^2), sum of squares of the errors (SSE), average relative error (ARE), residual root mean square error (RMSE), coefficient of determination (R^2), standard deviation of relative errors (S_{RE}), Marquardt's percentage standard deviation (MPSD), normalized standard deviation (NSD), hybrid functional error (HYBRID), sum of absolute error (EABS) and Spearman's correlation coefficient (r_s) error functions. These error functions were minimized while R^2 was maximized simultaneously over examined concentration range to obtain best experimental data fitness and estimation of models coefficients using Microsoft Excel® solver Add-Ins.

The global increase in the demand for brilliant green dye is becoming alarming due to its verse usage in many industries aiming at meeting human demands despite the exponential increase in World population on yearly basis. In achieving this, the water bodies are polluted with toxic and carcinogenic constituents of the dye when discharged as waste effluents from the industries. This is detrimental to humans' health and also constitute nuisance into the environment. Thus, there is need to design a low-cost adsorption column as part of waste treatment plant to remove these deadly constituents from aqueous solution before being discharged into water bodies. To achieve this, isotherm parameters prediction are needed from already existing experimental data of executed laboratory work involving adsorption of BGD from aqueous solution. Not only this, a low-cost adsorbent that is environmentally friendly and readily available is required.

MATERIALS AND METHODS

This research study was conducted inside the Unit Operation and Material Science Laboratory of Chemical and Petroleum Engineering Department, Afe Babalola University, Ado-Ekiti, Ekiti State, Nigeria between 5th February, 2018 and 27th April, 2018.

SS-RH composite adsorbent preparation: The rice husk and snail shell were obtained as wastes from Lafenwa market, Abeokuta, Ogun state and Bodija international market, Ibadan, Oyo state, Nigeria, respectively. Both materials were oven dried at 100°C for 24 h after pre-treatment and grinded to obtain 0.4 mm particle size. Snail shell-rice husk mixing ratio of 2.61 was prepared with the addition of 100 mL distilled water in a beaker to form a suspension and filtered. The residue was placed in an oven to eliminate excess water for 2 h at a temperature of 130°C. The mixture was calcined at 681.10°C for 2.61 h in a muffle furnace (Carbolite, ELF11/6B, S/N 21-403009, United Kingdom) to obtain the composite adsorbent.

Adsorbate preparation: The physico-chemical properties of the purchased BGD (from TopJay Scientific Laboratory, Ajilosun, Ado-Ekiti, Ekiti state) were chemical formulae $C_{27}H_{33}N_2.HO_4S$, molar mass 482.64 g moL^{-1}, melting point 210°C, maximum wavelength 625 nm and solubility in water to be 100 g L^{-1} at 20°C. About 1 L of distilled water (1000 mg L^{-1}) was used to dissolve 1 g of brilliant green dye powder to make a stock solution.

Batch adsorption equilibrium studies: The batch adsorption process was executed using a temperature-controlled magnetic heat stirrer (Stuart heat-stirrer, SB162). UV-visible spectrophotometer (Spectrum lab 752s) was used to measure filtrate absorbance at maximum wavelength of 625 nm. A calibration curve was prepared by plotting absorbance measured at different initial concentrations of 20, 40, 60 and 80 mg L^{-1} of BGD against each other to determine adsorbate concentration. The adsorption capacity of the adsorbent, q_e (mg g^{-1}) at equilibrium is measured using Eq. 1:

$$q_e = (C_o - C_e)\frac{V}{W} \quad (1)$$

where, C_o and C_e are initial and final concentrations of the BGD (mg L^{-1}), V is the volume of solution (L) and W is the weight of adsorbent (g).

Characterization of material: The calcined particles of snail shell-rice husk used as adsorbent for BGD adsorption was characterized before and after the process using scanning electron microscopy (SEM-JEOL-JSM 7600F) to study its surface morphology and textural structure. The active functional groups present in the adsorbent enhancing its adsorptive characteristic for BGD uptake from aqueous solution was characterized by Fourier transform infrared (FTIR) spectrometer (Nicolet iS10 FT-IR Spectrometer).

Equilibrium adsorption isotherm models: Adsorption isotherms explain adsorbed molecules distribution between the liquid phase and the solid phase when the adsorption process reaches an equilibrium state. Table 1 summarized all the isotherm models used. The isotherm models used to fit the experimental data include two-parameters (Freundlich, Langmuir, Temkin, Dubinin-Radushkevich, Harkin-Jura and Halsey) and three-parameters (Redlich-Peterson, Sips and Toth) isotherm models.

Error functions: The list of error functions (non-linear chi-square test, sum of squares of the errors, average relative error, residual root mean square error, coefficient of determination, standard deviation of relative errors, Marquardt's percentage standard deviation, normalized standard deviation, hybrid functional error, sum of absolute error and Spearman's correlation coefficient) used for this study was presented in Table 2. Non-linear chi-square test is calculated via summation of squares differences between experimental and calculated data with each squared difference divided by its corresponding value. Sum of squares of the errors is obtained by summing the squares of the difference between experimental and calculated value for the number of data points considered. The residual root mean square error is used to judge equilibrium model with optimal magnitude. The coefficient of determination, R^2 gives the proportion of one variable variance that is predictable from the other variable and its measure allows validating the certainty of predictions made from a certain model. Hybrid functional error was developed as an improvement on sum of squares errors (SSE) at low concentrations obtained by dividing SSE value with the experimental solid-phase concentration with an inclusive divisor in the system as a term for the number of degrees of freedom (Data points number - the number of parameters within the isotherm equation). The algorithms for the simulation of linear and non-linear isotherm models using error functions with aide of Microsoft Excel® solver Add-Ins were presented as Fig. 1 and 2, respectively.

Table 1: Equilibrium isotherm models used for the BGD uptake onto SS-RH

	Two parameter isotherms				
Models	Linear models	Non-linear models	Plot	Slope and intercept	References
Freundlich	$\log q_e = \log K_F + \frac{1}{n}\log C_e$	$q_e = K_F C_e^{\frac{1}{n}}$	log q_e vs log C_e	Slope = 1/n, Intercept = log K_F	Piccin *et al.*[42]
Langmuir	$\frac{C_e}{q_e} = \frac{1}{K_L q_{max}} + \frac{C_e}{q_{max}}$, $R_L = \frac{1}{1+K_L C_o}$	$q_e = \frac{q_{max} K_L C_e}{1+K_L C_e}$	$\frac{C_e}{q_e}$ vs. C_e	$Slope = \frac{1}{q_{max}}$, $Intercept = \frac{1}{(K_L q_{max})}$	Langmuir[43]
Temkin	$q_e = b_T \ln A_T + b_T \ln C_e$	$q_e = \frac{RT}{b_T}\ln A_T C_e$	q_e vs ln C_e	Slope = b_T, Intercept = $b_T \ln A_T$	Temkin and Pyzhev[44]
Dubinin-Radushkevich	$\ln(q_e) = \ln(q_m) - B_D\varepsilon^2$, $\varepsilon = RT\ln\left(1+\frac{1}{C_e}\right)$, $E = \frac{1}{\sqrt{(-2B_D)}}$	$q_e = (q_m)\exp(-B_D\varepsilon^2)$	$\ln q_e$ vs. $\left[\ln\left(1+\frac{1}{C_e}\right)\right]^2$	Slope = $B_D (RT)^2$, Intercept = ln (q_m)	Dubinin[45], Hobson[46]
Harkin-Jura	$\frac{1}{q_e^2} = \frac{B_{HJ}}{A_{HJ}} - \left(\frac{1}{A_{HJ}}\right)\log C_e$	$q_e = \left(\frac{A_{HJ}}{B_{HJ} - \log C_e}\right)^{\frac{1}{2}}$	$\frac{1}{q_e^2}$ vs. log C_e	$Slope = -\left(\frac{1}{A_{HJ}}\right)$, $Intercept = \frac{B_{HJ}}{A_{HJ}}$	Almeida *et al.*[47]
Halsey	$\ln q_e = \frac{1}{n_H}\ln K_H - \frac{1}{n_H}\ln C_e$	$q_e = \exp\left(\frac{\ln K_H - \ln C_e}{n_H}\right)$	ln q_e vs. ln C_e	$Slope = -\frac{1}{n_H}$, $Intercept = \frac{1}{n_H}\ln K_H$	Tahir *et al.*[48]
	Three-parameter isotherms				
Models	Linear models	Non-linear models	Plot	Slope and intercept	References
Redlich-Peterson	$\ln\left(K_{RP}\frac{C_e}{q_e} - 1\right) = \beta_{RP}\ln C_e + \ln a_{RP}$	$q_e = \frac{K_{RP} C_e}{1 + a_{RP} C_e^{\beta_{RP}}}$	$\ln\left(K_{RP}\frac{C_e}{q_e} - 1\right)$ vs. $\ln C_e$	Slope = β_{RP}, Intercept = $\ln a_{RP}$	Redlich and Peterson[49]
Sips	$\ln\left(\frac{q_e}{q_m - q_e}\right) = \frac{1}{n}\ln(C_e) + \ln(b_s)^{\frac{1}{n}}$	$q_e = \frac{q_m b_s C_e^{\frac{1}{n}}}{\left(1 + b_s C_e^{\frac{1}{n}}\right)}$	$\ln\left(\frac{q_e}{q_m - q_e}\right)$ vs. $\ln C_e$	$Slope = \frac{1}{n}$, $Intercept = \ln(b_s)^{\frac{1}{n}}$	Sips[50]
Toth	$\ln\left(\frac{q_e^{n_t}}{q_m^{n_t} - q_e^{n_t}}\right) = n_t \ln C_e + n_t \ln K_t$	$q_e = \frac{q_m K_t C_e}{\left(1 + (K_t C_e)^{n_t}\right)^{\frac{1}{n_t}}}$	$\ln\left(\frac{q_e^{n_t}}{q_m^{n_t} - q_e^{n_t}}\right)$ vs. $\ln C_e$	Slope = n_t, Intercept = $n_t \ln K_t$	Toth[51]

q_e (mg g^{-1}): Experimental adsorption capacity of SS-RH adsorbent at equilibrium, K_F (mg g^{-1}) (L mg^{-1}): Freundlich isotherm constant related to the sorption capacity, (mg L^{-1}): BGD adsorbate equilibrium concentration, a constant which gives an idea of the grade of heterogeneity, (L mg^{-1}): Langmuir constant related to the affinity of the binding sites and the energy of adsorption, C_o (mg L^{-1}): Highest initial adsorbate concentration, R_L: Dimensionless Langmuir equilibrium parameter, (mg g^{-1}): Maximum monolayer adsorption capacity of the SS-RH adsorbent, (8.314 $Jmol^{-1}$): Universal gas constant, (°K): Absolute temperature, (J mol^{-1}): Temkin constant related to heat of adsorption, (L mg^{-1}): Equilibrium binding constant corresponding to the maximum binding energy, (mol^2 kJ^{-2}): Dubinin-Radushkevich isotherm constant of adsorption energy, Polanyi potential related to the equilibrium concentration, (kJ mol^{-1}): Mean free energy of adsorption, A_{HJ} and B_{HJ}: Harkin-Jurah adsorption constants; K_H and n_H: Halsey isotherm constants; K_{RP} (L g^{-1}): Redlich-Peterson isotherm constant, a_{RP} (L mg^{-1}): Redlich-Peterson isotherm constant, β: Redlich-Peterson exponent which lies between 0 and 1, b_s: Sips isotherm constant related to energy of adsorption, K_t: Toth model adsorption isotherm constant, n_t: Toth model exponent

Table 2: List of error functions

Error functions	Abbreviations	Models	References
Nonlinear chi-square test	χ^2	$\chi^2 = \sum_{i=1}^{n} \frac{\left(q_{e,exp} - q_{e,calc}\right)^2}{q_{e,exp}}$	Ho and ofomaja[52] and Boulinguiez *et al.*[53]
Sum of squares of the errors	SSE	$SSE = \sum_{i=1}^{n} \left(q_{e,exp} - q_{e,calc}\right)^2$	Kumar and Sivanesan[40]
Average relative error	ARE	$ARE = \frac{100}{n} \sum_{i=1}^{n} \left\lvert \frac{q_{e,exp} - q_{e,calc}}{q_{e,exp}} \right\rvert$	Subramanyam and Das[54]
Residual root mean square error	RMSE	$RMSE = \sqrt{\frac{1}{n-2} \sum_{i=1}^{n} \left(q_{e,exp} - q_{e,calc}\right)^2}$	Vijayaraghavan *et al.*[55]
Coefficient of determination	R2	$R^2 = \frac{\sum \left(q_{e,exp} - \bar{q}_{e,calc}\right)^2}{\sum \left(q_{e,exp} - \bar{q}_{e,calc}\right)^2 + \sum \left(q_{e,exp} - q_{e,cal}\right)^2}$	Marquardt[56]
Standard deviation of relative errors	SRE	$S_{RE} = \sqrt{\frac{\sum_{i=1}^{n} \left[\left(q_{e,exp} - q_{e,calc}\right) - ARE\right]^2}{n-1}}$	Marquardt[56]
Marquardt's percentage standard deviation	MPSD	$MPSD = 100 \sqrt{\frac{1}{n-p} \sum_{i=1}^{n} \left(\frac{q_{e,exp} - q_{e,calc}}{q_{e,exp}}\right)^2}$	Marquardt[56]
Normalized standard deviation	NSD	$NSD = \Delta q(\%) = 100 \sqrt{\frac{1}{n-1} \sum_{i=1}^{n} \left(\frac{q_{e,exp} - q_{e,calc}}{q_{e,exp}}\right)^2}$	Wang *et al.*[57]
Hybrid functional error	HYBRID	$HYBRID = \frac{100}{(n-p)} \sum_{i=1}^{n} \frac{\left(q_{e,exp} - q_{e,calc}\right)}{q_{e,exp}}$	Ng *et al.*[58]
Sum of absolute error	EABS	$EABS = \sum_{i=1}^{n} \left\lvert q_{e,exp} - q_{e,calc} \right\rvert$	Ng *et al.*[59]

$q_{e,exp}$(mg g^{-1}): Value obtained from the batch experiment, $_{calc}$ (mg g^{-1}): Calculated value from the isotherm for corresponding, $q_{e,exp}$, $\bar{q}_{calc}$ (mg g^{-1}): Mean of $q_{e,calc}$, n: Number of experimental data points and p: Number of parameters in the respective model

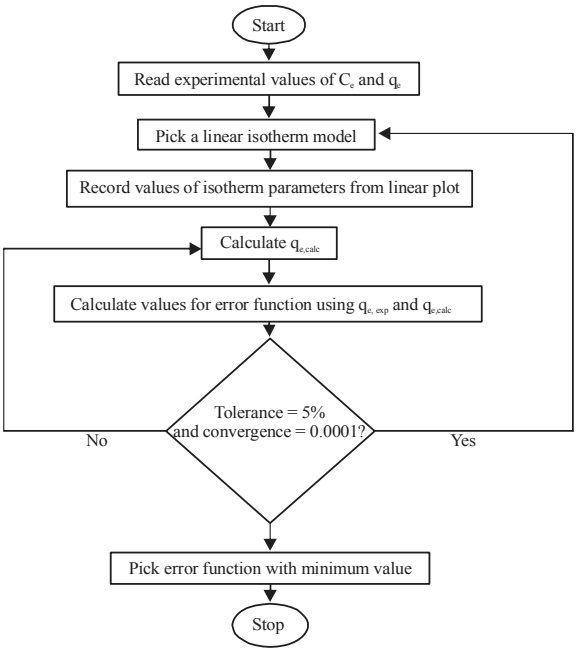

Fig. 1: Algorithm for linear isotherm models regression using error functions

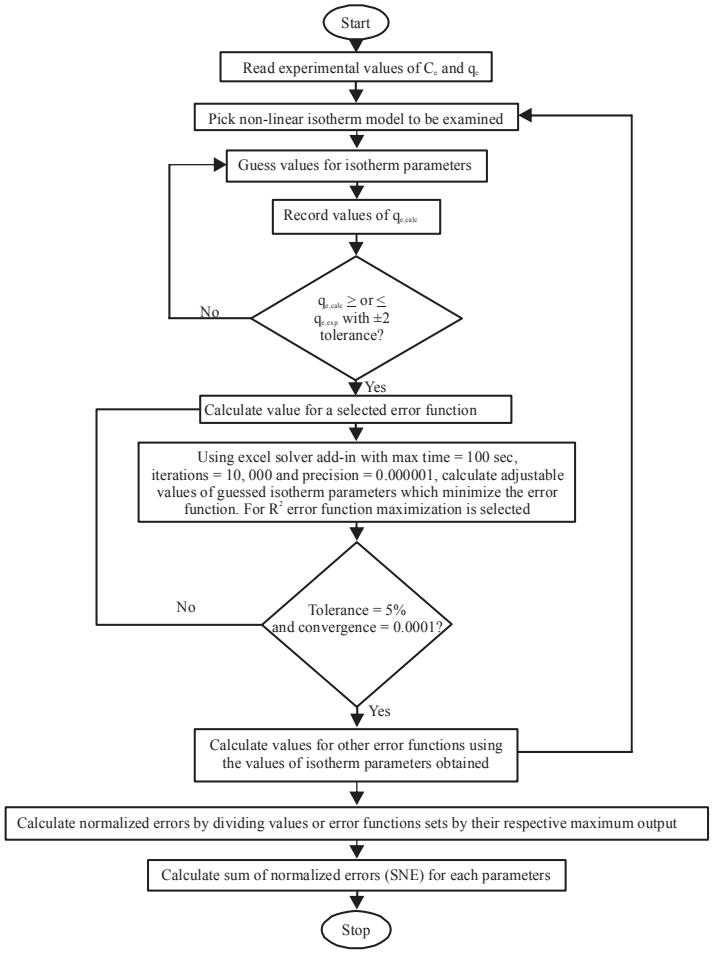

Fig. 2: Algorithm for non-linear isotherm models regression using error functions

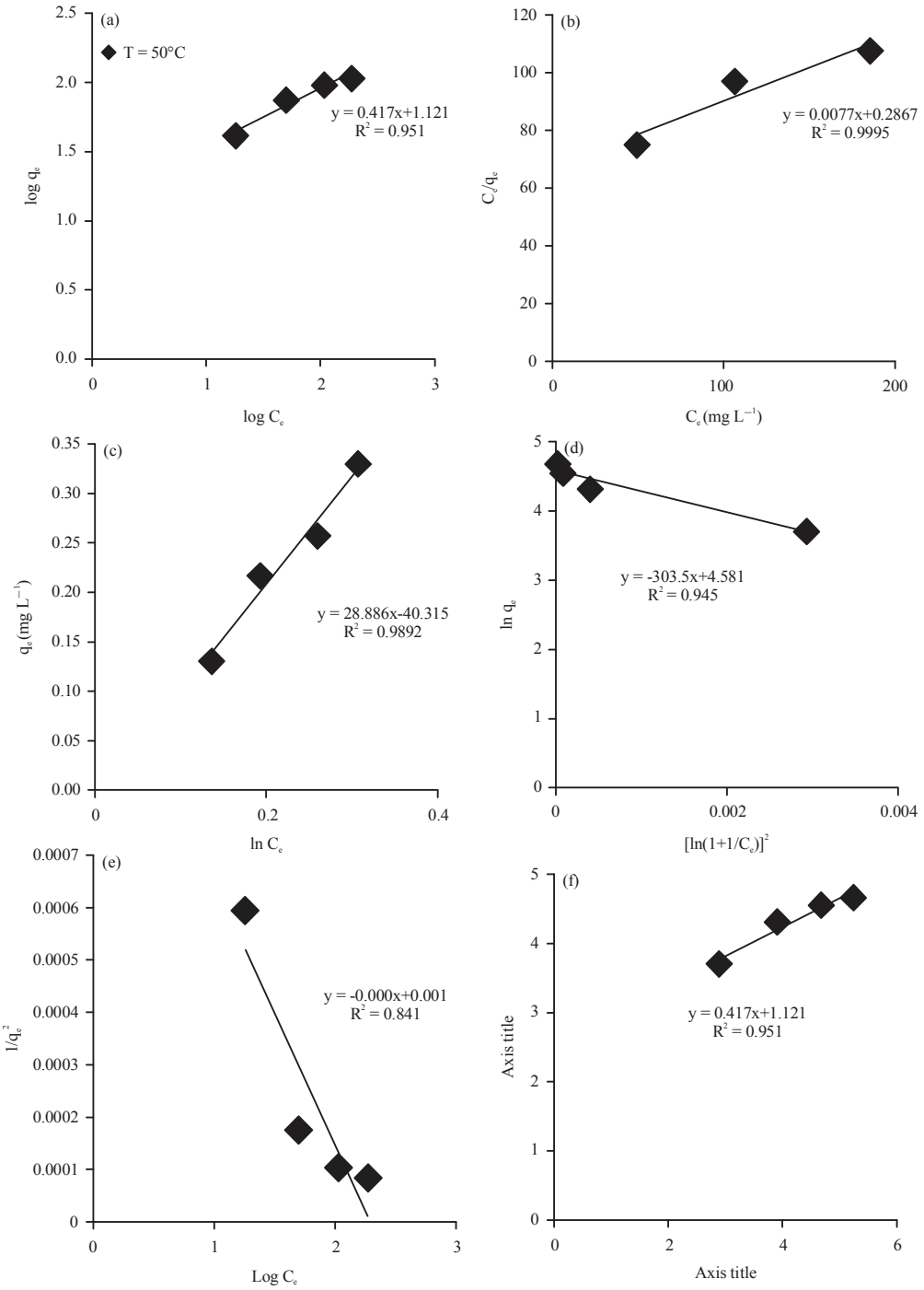

Fig. 3(a-f): Linearized two-parameter isotherm plots for (a) Freundlich (b) Langmuir (c) Temkin (d) Dubinin-Radushkevich (e) Harkin-Jura and (f) Halsey

RESULTS AND DISCUSSION

Linear regression of two-parameter isotherm models: Figure 3 presented linear plots for all the linearized two-parameter isotherm models for BGD uptake on SS-RH at 50°C. Among the investigated two-parameter isotherms, a value of 0.9995 obtained for R^2 by Langmuir isotherm proved it to be well-fitted for the BGD uptake onto SS-RH. In support of this, maximum monolayer adsorbent capacity q_{max} value of 129.87 mg g^{-1} was predicted by Langmuir

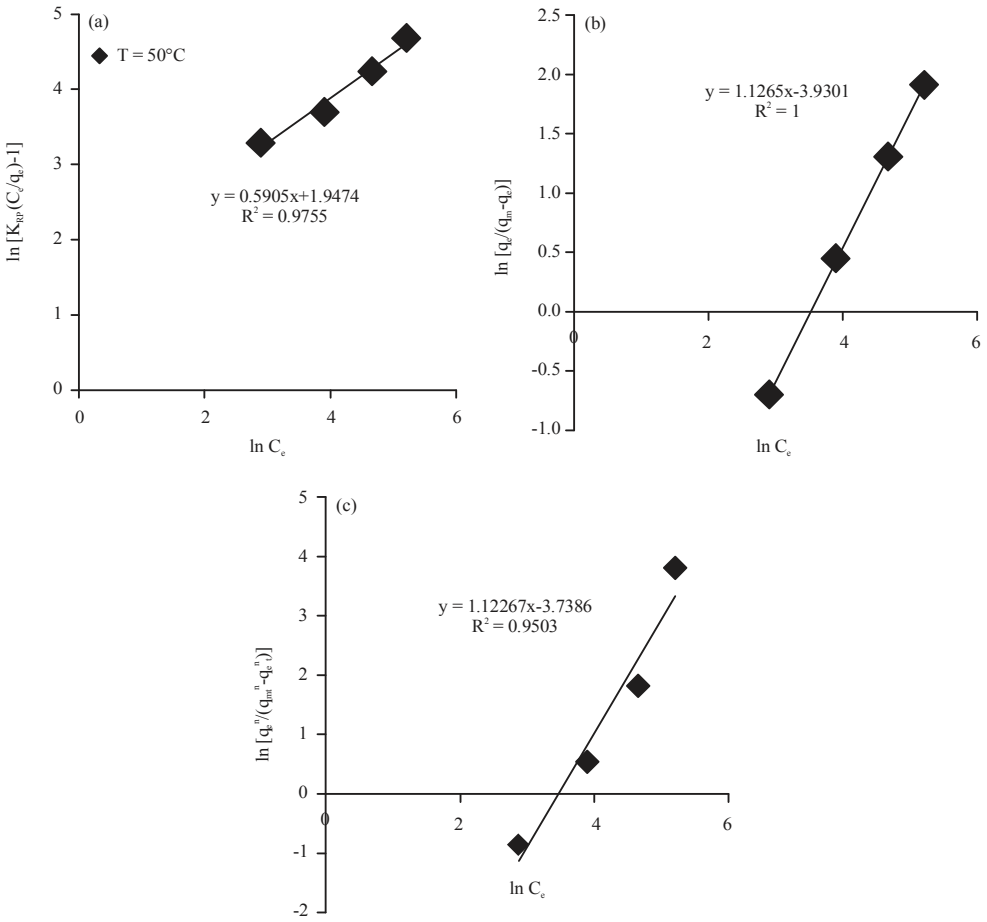

Fig. 4(a-c): Linearized three-parameter isotherm plots for (a) Redlich-Peterson (b) Sips and (c) Toth

Table 3: Non-linear two-parameter adsorption isotherm constants based on minimum SNE and R^2 values for BGD uptake on SS-RH at 50°C

	Freundlich			Langmuir			Temkin	
K_F [(mg g^{-1})(L mg^{-1})$^{1/n}$]	1/n	R^2	q_{max} (mg g^{-1})	K_L (L mg^{-1})	R^2	b_T (kJ mol^{-1})	A_T (L mg^{-1})	R^2
13.0406	0.4180	0.9365	131.1093	0.0260	0.9983	85.4446	0.2046	0.9802
	Dubinin-Radushkevich			Harkin-Jura			Halsey	
q_{max} (mg g^{-1})	$B_D \times 10^{-5}$ (mol^2 kJ^{-2})	R^2	A_{HJ}	B_{HJ}	R^2	n_H	K_H	R^2
97.8204	4.3274	0.9157	2948.771	2.5227	0.0895	10.0805	1×10^{20}	0.4257

model. Similar results were presented by Kooh *et al.*[60] and Hamzaoui *et al.*[61] while Nethaji *et al.*[62] presented a contrary result.

Linear regression of three-parameter isotherm models: Figure 4 presented linear plots for all the linearized three-parameter isotherm models for BGD uptake on SS-RH at 50°C. The sip isotherm fitted well for the adsorption of BGD using SS-RH with R^2 value of 1.000. The R^2 values for Redlich-Peterson and Toth isotherms were 0.9755 and 0.9503, respectively. Similar result had been presented elsewhere[63].

Two-parameter isotherm models non-linear regression: The best fit was chosen based on sum of normalized error (SNE) with minimum value. Table 3 presented the values of isotherm constants and R^2 values obtained for each two-parameter isotherm models. The R^2 values revealed Langmuir to be two-parameter isotherm model that best describes adsorption of BGD onto SS-RH. The increasing order of best fit is Langmuir>Temkin>Freundlich>Dubinin-Radushkevich> Halsey>Harkin-Jura with R^2 values of 0.9983>0.9802> 0.9365> 0.9157>0.4257>0.0895 which is the same as that obtained for the linear regression. Nevertheless, values of isotherm constants obtained for the non-linear regression are very

Table 4: Non-linear three-parameter adsorption isotherm constants based on minimum SNE and R^2 values for BGD uptake on SS-RH at 50°C

Redlich-Peterson				Sips				Toth			
K_{RP} (L g^{-1})	a_{RP} (L mg^{-1})	β_{RP}	R^2	1/n	b_s (L g^{-1})	q_m (mg g^{-1})	R^2	n_t	K_t	q_m (mg g^{-1})	R^2
3.0366	0.0149	1.0892	0.9996	1.1432	0.0185	122.1850	0.9999	1.2584	0.0240	120.1149	0.9999

Table 5: Error functions for linear regression

	Error functions									
Models	R^2	χ^2	SSE	ARE	RMSE	S_{RE}	MPSD	NSD	HYBRID	EABS
Two-parameters isotherm models										
Freundlich	0.9362	2.0628	175.9846	7.8095	9.3804	11.8105	11.4960	9.3865	15.6190	24.5745
Langmuir	0.9984	0.0770	4.1280	1.5594	1.4367	2.3216	2.8354	2.3151	3.1188	3.7698
Temkin	0.9893	0.3743	27.9383	3.6273	3.7375	5.2184	5.3996	4.4088	7.2547	10.4705
D-R	0.9143	2.7626	241.9271	7.0652	10.9983	11.7803	12.7627	10.4207	14.1305	24.2266
H-J	0.8617	5.0446	422.7903	12.5909	14.5394	21.8056	18.1083	14.7854	25.1818	39.4935
Halsey	0.9325	2.1602	186.9215	7.9017	9.6675	12.8670	11.8114	9.6439	15.8033	24.5931
Three-parameters isotherm models										
R-P	0.7039	38.4831	3347.5980	34.0905	40.9121	13.0308	68.9862	39.8292	136.3618	109.8080
Sips	0.9999	0.0028	0.2185	0.2892	0.3306	0.5713	0.6549	0.3781	1.1566	0.8494
Toth	0.8752	8.0441	389.1901	14.6936	13.9497	19.0037	42.1909	24.3589	58.7745	32.1797

close to those of linear regression which shows the efficacy of the non-linear isotherm models. Kooh *et al.*[60] presented similar result while a contrary result was exhibited by Ozdemir and Keskin[64].

Three-parameter isotherm models non-linear regression: The sum of normalized error with minimum value was also used here in selecting the best fit for the non-linear regression of three-parameter isotherm models. The values of isotherm constants and R^2 values obtained are presented in Table 4 while the plots of adsorbed quantity of BGD by calcined SS-RH particles (q_e) with initial BGD concentrations (C_e) for all the three-parameter isotherm models are shown in Fig. 5. Sips and Toth are the best fit with R^2 value of 0.9999. This was also supported by Dahri *et al.*[63] and Verma *et al.*[65]. In all the plots shown in Fig. 5, L-type shape indicates that adsorbed quantity of BGD onto SS-RH increases with BGD initial concentration[66]. Nevertheless, it shows the efficacy of the calcined SS-RH adsorbent to adsorb BGD even at higher initial concentrations. This is also supported by increased in driving force for mass transfer at higher concentrations[67,68].

Error functions for linear fit: Table 5 presented the values obtained from the simulation of error functions using linearized isotherm models of two and three parameters. The result revealed Langmuir isotherm model to be the best two-parameter model fit for BGD uptake from aqueous solution using SS-RH having highest R^2 value of 0.9984 and lowest values for the error functions while Sips is the best three-parameter isotherm model that best describes the adsorption process with highest R^2 value of 0.9999 and lowest error functions values. The order of best fit for two-parameter isotherm models is Langmuir Temkin

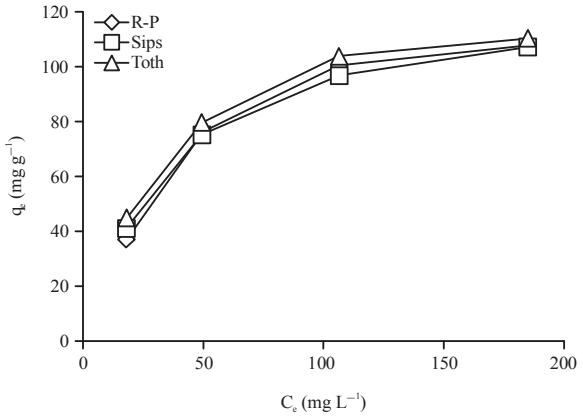

Fig. 5: Non-linearized regression of three-parameter isotherm models for BGD adsorption onto SS-RH

Freundlich Halsey D-R H-J while the order is Sips Toth R-P for three-parameter models. Nevertheless, of all the error functions used, chi-square was the best error method that can accurately determine isotherm model parameters as it gave the lowest error value of 0.0770 and 0.0028 for two and three-parameters isotherm models, respectively[69]. The error functions results also corroborate with the linear regression analysis for the isotherm models as both Langmuir and Sips were revealed to be the best model describing BGD adsorption from aqueous solution using SS-RH composite adsorbents. Previous studies have also presented similar results[70,71].

Error functions for non-linear fit

Two-parameter isotherm models: The results of different error functions used for the non-linear regression of two and three-parameter isotherm models are presented in Table 6.

Table 6: Error functions for non-linear regression

	Non-linear freundlich isotherm (Two-parameters)									
Models	R^2	χ^2	SSE	ARE	RMSE	S_{RE}	MPSD	NSD	HYBRID	EABS
K_F	16.8110	14.6012	16.8044	14.5942	16.8043	12.7044	13.0406	13.0405	16.8000	16.8101
1/n	0.3636	0.3934	0.3637	0.3824	0.3637	0.4052	0.4180	0.4180	0.3555	0.3553
R^2	0.9510	0.9465	0.9510	0.9250	0.9510	0.8887	0.9365	0.9365	0.9376	0.9376
χ^2	2.1612	1.9236	2.1595	2.6788	2.1595	4.1356	2.0641	2.0642	2.4844	2.4848
SSE	132.9008	145.8949	132.9002	215.2372	132.9002	348.1378	175.1534	175.1561	173.6063	173.4964
ARE	8.6888	8.1153	8.6865	7.8935	8.6865	8.2587	7.7272	7.7272	8.5183	8.5212
RMSE	8.1517	8.5409	8.1517	10.3739	8.1517	13.1935	9.3582	9.3583	9.3168	9.3139
S_{RE}	12.2647	11.2266	12.2510	8.0277	12.2510	7.1501	11.0980	11.0981	9.7000	9.7086
MPSD	14.2800	11.9961	14.2685	13.2703	14.2685	15.7961	11.4238	11.4239	14.2102	14.2189
NSD	11.6596	9.7948	11.6502	10.8351	11.6502	12.8975	9.3275	9.3275	11.6026	11.6097
HYBRID	17.3777	16.2306	17.3731	8.2302	17.3731	16.5175	1.3052	1.3053	17.0367	2.4828
EABS	22.7673	23.7201	22.7690	23.3701	22.7690	28.3091	24.6054	24.6056	22.5702	22.5670
SNE	8.134475	7.666938	8.131014	7.567282	8.131014	9.418471	6.881162	6.881230	8.139603	7.303683
Non-linear Langmuir isotherm (Two-parameters)										
q_{max}	130.1184	131.1093	130.1183	134.0179	130.1183	130.0548	132.0671	132.0671	132.0671	127.6149
K_L	0.0267	0.0260	0.0267	0.0245	0.0267	0.0256	0.0254	0.0254	0.0250	0.0288
R^2	0.9984	0.9983	0.9984	0.9965	0.9984	0.9960	0.9979	0.9979	0.9972	0.9972
χ^2	0.0697	0.0620	0.0697	0.0988	0.0697	0.1275	0.0669	0.0669	0.0893	0.1710
SSE	4.0577	4.4853	4.0577	9.0354	4.0577	10.2702	5.5016	5.5016	7.2620	7.2526
ARE	1.5180	1.4061	1.5180	1.1774	1.5180	1.3674	1.3175	1.3175	1.2432	1.8453
RMSE	1.4244	1.4975	1.4244	2.1255	1.4244	2.2661	1.6586	1.6586	1.9055	1.9043
S_{RE}	2.1886	2.0182	2.1884	2.2732	2.1884	1.3348	2.0077	2.0077	1.6754	3.0114
MPSD	2.6067	2.1981	2.6066	2.3610	2.6066	2.8297	2.0904	2.0904	2.3643	4.5319
NSD	2.1284	1.7947	2.1283	1.9277	2.1283	2.3105	1.7068	1.7068	1.9304	3.7003
HYBRID	3.0359	2.8122	3.0359	2.3548	3.0359	2.7347	2.6349	2.6349	2.4864	3.6907
EABS	3.8292	3.9651	3.8293	4.2383	3.8293	4.5356	4.0697	4.0697	4.2683	3.5045
SNE	6.797889	6.498436	6.797796	7.400936	6.797796	7.917252	6.572740	6.572740	6.957199	9.317985
Non-linear Temkin isotherm (Two-parameters)										
b_T	92.9657	90.6904	92.9657	86.2552	92.9658	94.1191	89.0458	89.0458	89.0458	85.4446
A_T	0.2477	0.2307	0.2477	0.2107	0.2477	0.2335	0.2206	0.2206	0.2161	0.2046
R^2	0.9893	0.9887	0.9893	0.9814	0.9893	0.9788	0.9874	0.9874	0.9869	0.9802
χ^2	0.3727	0.3417	0.3727	0.4828	0.3728	0.6732	0.3560	0.3560	0.3824	0.5110
SSE	27.9323	29.5691	27.9323	49.1090	27.9323	56.5742	32.8848	32.8848	34.2220	52.1184
ARE	3.6174	3.1797	3.6174	2.6284	3.6175	3.1506	2.8956	2.8956	2.7411	2.4217
RMSE	3.7371	3.8451	3.7371	4.9553	3.7371	5.3186	4.0549	4.0549	4.1366	5.1048
S_{RE}	5.1728	4.7553	5.1728	5.8280	5.1730	3.1244	4.7331	4.7331	4.1463	5.6542
MPSD	5.3694	4.6310	5.3694	4.9408	5.3696	6.3775	4.4894	4.4894	4.6869	5.0500
NSD	4.3841	3.7812	4.3841	4.0341	4.3843	5.2072	3.6655	3.6655	3.8268	4.1233
HYBRID	7.2349	6.3593	7.2349	5.2567	7.2350	6.3011	5.7912	5.7912	5.4821	4.8434
EABS	10.4704	10.1401	10.4704	9.4461	10.4704	10.6318	9.8908	9.8908	9.8908	9.3114
SNE	8.306214	7.732511	8.306214	8.399985	8.306508	9.267340	7.621757	7.621757	7.575291	8.399462
Non-linear Dubinin-Radushkevich isotherm (Two-parameters)										
q_{max}	99.5280	97.8204	99.5280	99.3553	99.5239	87.0231	96.1365	96.1027	99.3247	101.2865
$B_D \times 10^{-5}$	4.6418	4.3274	4.6337	4.2021	4.6385	5.0114	4.1411	4.1395	4.2025	4.2959
R^2	0.9183	0.9157	0.9183	0.9144	0.9183	0.8090	0.9093	0.9091	0.9144	0.9110
χ^2	2.8724	2.7410	2.8675	2.8937	2.8702	8.6404	2.8220	2.8247	2.8893	3.1665
SSE	229.5278	237.8142	229.5287	241.9766	229.5272	726.1105	258.3910	258.8829	241.8134	254.0987
ARE	8.1621	7.5395	8.1281	6.3413	8.1498	14.7114	7.4425	7.4501	6.3370	6.8173
RMSE	10.7128	10.9045	10.7128	10.9995	10.7128	19.0540	11.3664	11.3772	10.9958	11.2716
S_{RE}	12.6733	11.8799	12.6706	12.2446	12.6744	9.6877	11.3916	11.3841	12.2209	13.6736
MPSD	13.8847	12.8393	13.8592	13.3145	13.8784	24.9099	12.6253	12.6253	13.2998	14.1616
NSD	11.3368	10.4833	11.3160	10.8712	11.3317	20.3388	10.3085	10.3085	10.8592	11.5629
HYBRID	0.7330	0.4259	0.6305	12.6827	16.2996	29.4229	14.8850	14.9001	12.6739	13.63461
EABS	24.3343	24.8338	24.2748	21.7691	24.3104	44.5320	26.0971	26.1367	21.7852	23.0323
SNE	5.378589	5.198526	5.368649	5.556628	5.905602	9.589472	5.713813	5.716522	5.552557	5.881071
Non-linear Harkin-Jura isotherm (two-parameters)										
A_{HJ}	2916.173	3562.569	3513.921	3449.999	3399.821	2093.840	2948.771	2948.771	2948.771	2948.771
B_{HJ}	2.34×10^5	2.5449	2.82×10^5	2.5661	2.73×10^5	2.5016	2.4913	2.4913	2.5227	2.5227
R^2	0.9162	0.0840	0.9162	0.0863	0.9162	0.1165	0.0857	0.0857	0.0895	0.0895
χ^2	319.6541	7.0599	319.6541	7.5564	319.6541	18.9849	7.8099	7.8099	8.5318	8.5318
SSE	2580.4950	28267.9500	2580.4900	28267.9500	2580.4910	28267.8900	28267.9400	28267.9400	28267.9300	28267.9300
ARE	99.8399	15.5107	99.8399	14.7480	99.8399	18.9476	15.7140	15.7140	14.6957	14.6957
RMSE	35.9200	118.8864	35.9199	118.8864	35.9199	118.8863	118.8864	118.8864	118.8864	118.8864
S_{RE}	37.1976	20.1313	37.1976	16.8878	37.1976	13.6110	19.0463	19.0463	15.5278	15.5278
MPSD	141.1950	24.7931	141.1950	24.5544	141.1950	33.0002	23.4050	23.4050	24.0559	24.0559
NSD	115.2853	20.2435	115.2853	20.0486	115.2853	26.9445	19.1101	19.1101	19.6416	19.6416
HYBRID	199.6799	31.0213	199.6799	29.4960	199.6799	37.8953	31.4280	31.4280	29.3914	29.3914
EABS	320.1002	41.8594	320.1002	39.5225	320.1002	67.6869	46.7383	46.7383	42.5692	42.5692
SNE	8.393424	3.447638	8.393423	3.338546	8.393423	3.610912	3.422323	3.422323	3.309937	3.309937

Table 6: Error functions for non-linear regression

	Non-linear freundlich isotherm (Two-parameters)									
Models	R^2	χ^2	SSE	ARE	RMSE	S_{RE}	MPSD	NSD	HYBRID	EABS
Non-linear Halsey isotherm (Two-parameters)										
n_H	5.41×10^{8}	10.0805	9.6941	9.7544	9.6660	12.2371	10.5503	10.5503	9.7544	9.7544
K_H	1.0×10^{20}	1.0×10^{20}	1.0×10^{20}	1.0×10^{20}	1.0×10^{20}	1.0×10^{20}	1.0×10^{20}	1.0×10^{20}	1.0×10^{20}	1.0×10^{20}
R^2	0.500	0.4257	0.3852	0.4544	0.3826	0.4907	0.4589	0.4589	0.3913	0.3913
χ^2	312.6043	62.0665	70.5855	67.8975	72.0597	132.3204	69.5309	69.5309	67.8975	67.8975
SSE	27630.970	4890.0400	4254.551	4286.399	4250.795	12815.2600	6475.5020	6475.5020	4286.399	4286.3990
ARE	98.5672	43.3621	43.866	42.6491	44.4522	54.7047	44.2178	44.2178	42.6491	42.6491
RMSE	117.5393	49.4472	46.1224	46.2947	46.1020	80.0477	56.9012	56.9012	46.2947	46.2947
S_{RE}	36.9262	47.6276	58.6866	55.7017	60.1522	32.4637	39.7980	39.7980	55.7017	55.7017
MPSD	139.3976	69.2279	83.7700	80.7604	85.2771	83.6452	64.1482	64.1482	80.7603	80.7603
NSD	113.8177	56.5244	68.3979	65.9406	69.6285	68.2960	52.3768	52.3768	65.9405	65.9405
HYBRID	197.1344	10.2201	87.7323	85.2983	88.9043	109.4093	88.4355	88.4355	85.2983	85.2983
EABS	316.5470	127.3641	112.2073	111.4226	112.5861	197.6429	145.5357	145.5357	111.4226	111.4226
SNE	9.613880	4.326761	4.964644	4.977089	5.022927	6.023670	4.797641	4.797641	4.850888	4.850888
Non-linear Redlich-Peterson isotherm (Three-parameters)										
K_{RP}	3.0873	3.0583	3.0873	3.4778	3.0876	3.0704	3.0396	3.0395	3.0363	3.0366
a_{RP}	0.0154	0.0147	0.0154	0.0356	0.0154	0.0154	0.0142	0.0142	0.0143	0.0149
β_{RP}	1.0804	1.0868	1.0804	0.9367	1.0804	1.0791	1.0918	1.0918	1.0893	1.0892
R^2	0.9998	0.9998	0.9998	0.9883	0.9998	0.9996	0.9998	0.9998	0.9998	0.9996
χ^2	0.0058	0.0054	0.0058	0.3183	0.0058	0.0114	0.0056	0.0056	0.0067	0.0066
SSE	0.4403	0.4646	0.4403	30.4853	0.4403	0.9410	0.5116	0.5120	0.6110	0.6118
ARE	0.4305	0.3821	0.4304	2.1645	0.4310	0.3953	0.3581	0.3579	0.3077	0.3068
RMSE	0.4692	0.4820	0.4692	3.9042	0.4692	0.6859	0.5058	0.5060	0.5527	0.5529
S_{RE}	0.6393	0.5898	0.6391	4.3220	0.6410	0.4122	0.5820	0.5821	0.6325	0.6334
MPSD	0.9238	0.8133	0.9232	5.8540	0.9257	1.1842	0.7936	0.7936	0.8653	0.8659
NSD	0.5333	0.4696	0.5330	3.3798	0.5345	0.6837	0.4582	0.4582	0.4996	0.4989
HYBRID	1.7220	1.5283	1.7216	8.6580	1.7239	1.5813	ch1.4325	1.4314	1.2308	1.2316
EABS	1.2464	1.2296	1.2465	7.7766	1.2459	1.3527	1.2386	1.2383	1.0878	1.0827
SNE	2.174416	2.081165	2.174099	9.988498	2.175875	2.281331	2.059893	2.059722	2.048831	2.047518
Non-linear Sips isotherm (Three-parameters)										
1/n	1.1395	1.1416	1.1395	1.1395	1.1395	1.1385	1.1432	1.1432	1.1432	1.1395
b_s	0.0187	0.0186	0.0187	0.0187	0.0187	0.0187	0.0185	0.0185	0.0185	0.0187
q_m	122.3609	122.2639	122.3609	122.3605	122.3605	122.2555	122.1850	122.1850	122.1850	122.3606
R^2	1.0000	0.9999	0.9999	0.9999	1.0000	0.9999	0.9999	0.9999	0.9999	0.9999
χ^2	0.000423	0.000408	0.000423	0.000463	0.000423	0.001148	0.000415	0.000415	0.000417	0.000463
SSE	0.0371	0.0381	0.0371	0.0405	0.0371	0.0990	0.0399	0.0399	0.0400	0.0405
ARE	0.1079	0.0963	0.1079	0.0965	0.1079	0.1471	0.0905	0.0905	0.0882	0.0965
RMSE	0.1363	0.1379	0.1363	0.1423	0.1363	0.2225	0.1413	0.1413	0.1414	0.1423
S_{RE}	0.1683	0.1582	0.1682	0.1382	0.1682	0.1227	0.1555	0.1555	0.1496	0.1382
MPSD	0.2257	0.2117	0.2256	0.2327	0.2256	0.3729	0.2092	0.2092	0.2101	0.2327
NSD	0.1303	0.1222	0.1303	0.1344	0.1303	0.2153	0.1208	0.1208	0.1213	0.1344
HYBRID	0.4317	0.3853	0.4315	0.3860	0.4317	0.5885	0.3618	0.3618	0.3529	0.3860
EABS	0.3508	0.3377	0.3507	0.3442	0.3508	0.4774	0.3325	0.3325	0.3313	0.3442
SNE	6.768145	6.451951	6.766633	6.554187	6.767283	9.728955	6.372008	6.372008	6.311617	6.554187
Non-linear Toth isotherm (Three-parameters)										
n_t	1.2435	1.2521	1.2435	1.2687	1.2435	1.2392	1.2584	1.2584	1.2063	1.2286
K_t	0.0242	0.0241	0.0242	0.0239	0.0242	0.0242	0.0240	0.0240	0.0239	0.0241
q_m	120.5514	120.3080	120.5517	120.0994	120.5515	120.4588	120.1148	120.1149	123.0771	121.0800
R^2	0.9999	0.9999	0.9999	0.9998	0.9999	0.9998	0.9999	0.9999	0.9995	0.9999
χ^2	0.001565	0.001486	0.001565	0.002666	0.001565	0.003033	0.001521	0.001521	0.012901	0.002588
SSE	0.1308	0.1353	0.1308	0.2581	0.1308	0.2596	0.1442	0.1442	1.2939	0.2013
ARE	0.2166	0.1913	0.2164	0.1314	0.2166	0.2164	0.1785	0.1785	0.4791	0.1946
RMSE	0.2557	0.2601	0.2557	0.3592	0.2557	0.3603	0.2685	0.2685	0.8043	0.3172
S_{RE}	0.3297	0.3061	0.3296	0.3919	0.3297	0.2281	0.3002	0.3002	1.0611	0.2627
MPSD	0.4504	0.4108	0.4502	0.5248	0.4504	0.6035	0.4040	0.4039	1.1407	0.5790
NSD	0.2600	0.2372	0.2599	0.3030	0.2600	0.3485	0.2332	0.2332	0.6586	0.3343
HYBRID	0.8662	0.7650	0.8657	0.5256	0.8662	0.8654	0.7141	0.7140	1.9162	0.7782
EABS	0.6732	0.6504	0.6730	0.5087	0.6732	0.7570	0.6433	0.6432	1.8499	0.6426
SNE	3.908702	3.702006	3.907494	3.965639	3.908702	4.469293	3.647328	3.647134	9.999599	4.172974

NB: Bolded values are the lowest values of respective error functions. Only R^2 have highest values

Among the two-parameter isotherm models studied, chi-square (χ^2) revealed parameter set with minimum SNE (6.4984, 5.1985 and 4.3268) in three out of the six models investigated. Thus, χ^2 proved to be the best predictive error function for the two-parameter isotherm study of BGD adsorption onto SS-RH. However, highest R^2 value of 0.9984

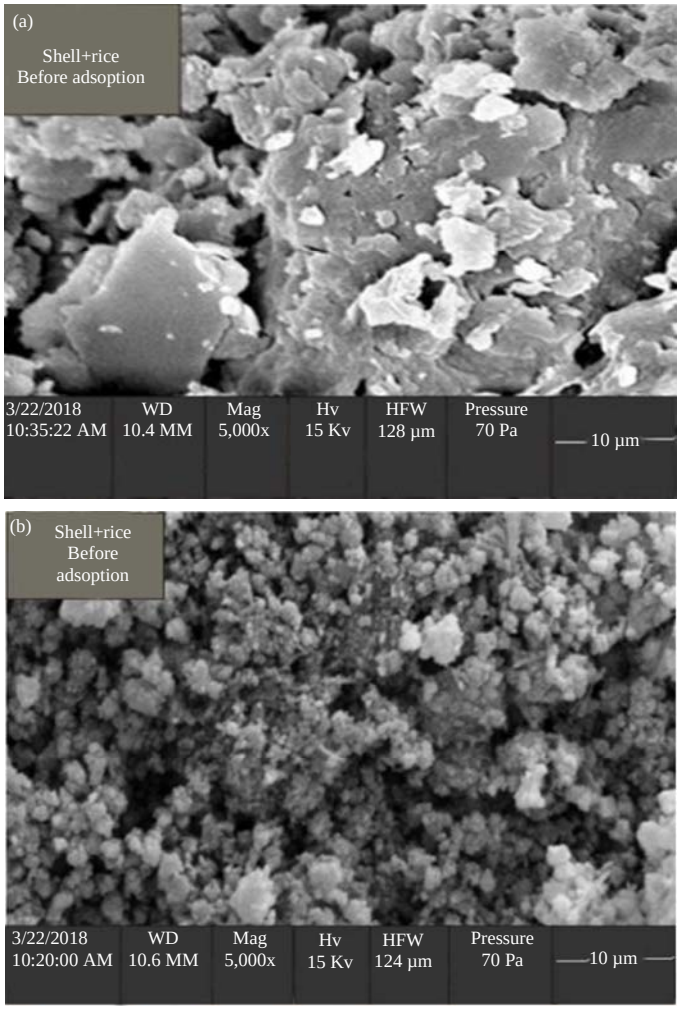

Fig. 6(a-b): SEM image of synthesized snail shell-rice husk (a) Composite adsorbent before and (b) After BGD adsorption

revealed non-linear Langmuir isotherm model to be the best fit for the adsorption process. In comparison with linear fit, same values were approximately obtained for R^2, q_{max} and K_L which shows a strong correlation. Similar result that affirms this outcome was presented by Ghaffari *et al.*[72].

Three-parameter isotherm models: For the non-linear three-parameter isotherm models, the result Table 6 revealed EABS, HYBRID and NSD as best error function for non-linear Redlich-Peterson, Sips and Toth isotherm models, respectively with respective lowest SNE values of 2.0475, 6.3116 and 3.6471. In comparison with linear fit, smaller SNE values show for non-linear isotherm models indicate linear isotherm transformation is not an appropriate method in selecting a model for BGD sorption equilibria using SS-RH. However, the R^2 error function results exhibited non-linear Sips isotherm model proved most appropriate three-parameter isotherm model for BGD adsorption using SS-RH with R^2 excellently equals to 1. Same values were approximately obtained for 1/n, b_s and q_{max} as linearized Sips isotherm model. This affirms the consistency of the non-linear Sips isotherm model with the linear form. Similar studies have also presented similar results[73,74].

Material characterization

SEM images: The SEM images obtained before and after the adsorption of BGD onto calcined particles of SS-RH are presented as Fig. 6(a, b), respectively. Figure 6a revealed an irregular surface texture with creation of pores resulting from the calcination of the raw composite adsorbent coupled with water liberation which allows uptake of BGD onto the surface and the pores. The SEM image shown in Fig. 6b which revealed the adsorption of BGD onto the surface and opening pores of the SS-RH. Nearly all the available pores created were

Table 7: FTIR of SS-RH before and after BGD adsorption

	FT-IR wavelength (cm^{-1}) for SS-RH		
IR band	Before adsorption	After adsorption	Observations/Suggestions
1	3761.41, 3691.66	-	Stretching vibration of H_2O
2	3442.00	3441.00	-OH and -NH functional groups vibration
3	2926.82	2969.96, 2929.20	Asymmetric stretching vibrations of the C-H bonds of the aliphatic groups
4	2869.54	2870.92	Symmetric stretching of C-H bond
5	2517.14	2517.24	Bending vibration of C-H bond in methylene group
6	1798.72	1799.38	Stretching vibration of -C = O of carboxylate groups
7	1427.63	1427.00	Aromatic rings vibrational stretching
8	872.86	872.86	S=O stretching bands of $-SO_3^-$ bonds in sulfonate groups
9	707.82	707.79	Out-of-plane bending of C-O
10	-	366.38	Bending vibration of Al-O-Si present in the rice husk

Table 8: Energy dispersive spectroscopy (EDS) of SS-RH adsorbent showing weight percentage of elements before and after adsorption

Elements	Wt. before adsorption (%)	Wt. after adsorption (%)
Sulphur	2.30	2.20
Oxygen	45.00	41.03
Aluminium	1.25	1.05
Sodium	3.70	5.10
Silicon	32.20	30.10
Calcium	10.21	15.00
Iron	3.11	3.12
Potassium	2.23	2.40

filled up with the BGD after the adsorption process with noticeable change in the colour of the calcined particles of SS-RH.

FT-IR analysis: Table 7 summarized the values of broad peaks wavelengths with respective suggestions revealed by FT-IR spectra of the composite SS-RH adsorbent before and after the uptake of BGD, respectively recorded in the range of 350-4400 nm. Observed sharp broad peaks suggested complex nature of the calcined particles of SS-RH adsorbent with the availability of active functional groups enhancing BGD adsorption onto the adsorbent surface and pores. A shift in the broad peaks of the spectrum after adsorption and the stated observations suggests functional groups presence on the SS-RH surface[32] and interaction between the BGD molecules and the functional groups during adsorption, respectively[60].

Energy dispersive spectroscopy (EDS) analysis: Table 8 presented the energy dispersive spectroscopy (EDS) results revealing formation of active mixed metal oxides (Al-O, Na-O, Fe-O, Ca-O, Si-O, S-O) with different weight percent due to calcination of the SS-RH particles at higher temperature. Changes in the respective weight of the active mixed metal oxides after adsorption revealed their positive influence on the BGD adsorption on the active sites of calcined SS-RH particles. A study also revealed silicon and calcium composition to be 32.2 and 10.21 wt% whose sources were from rice husk and snail shell, respectively[75]. Reduction in wt% of active oxides of Si, Al and S in the calcined SS-RH particles suggested their strong affinity to adsorb BGD from aqueous solution. Though a study presented by Kumar *et al.*[76] synthesized active mixed metal oxides from only rice husk for adsorption of cadmium from aqueous solution, similar weight percent were observed before and after the process.

CONCLUSION

Linear and non-linear regression of isotherm models having two and three parameters have been investigated using different error functions for BGD removal from aqueous solution using snail shell-rice husk. Langmuir and Sip fitted well for BGD uptake from aqueous solution using SS-RH. Chi-square (χ^2) predicted well for non-linear Langmuir model while EABS, HYBRID and NSD predicted well for non-linear R-P, Sips and Toth isotherm models for BGD adsorption onto SS-RH. The SEM images revealed formation of irregular surface texture with adsorbed BGD onto pore openings confirming SS-RH efficacy for the adsorption process. The FTIR exhibited shift in the spectrum broad peaks after adsorption. The EDS revealed formation of active mixed metal oxides after calcination.

SIGNIFICANCE STATEMENT

Though the use of rice husk as adsorbents for acidic dye is not a new development, this study unveils the efficacy of composite snail shell-rice husk for brilliant green dye adsorption from aqueous solution which is a readily available low-cost adsorbent that could be beneficial to small scale industries for waste water treatment before disposal. Also, this research work unveils not only best-fit isotherm model for the obtained experimental data but also best error function that gives highest efficiency of experimental data. These will be of enormous benefits to prospective researchers in the fields of equipment design (adsorption column) for waste water treatment and material science with specialization on generating useful materials from dumped wastes such that new theories and innovations can be developed in these areas of research.

REFERENCES

1. Gupta, G.S., S.P. Shukla, G. Prasad and V.N. Singh, 1992. China clay as an adsorbent for dye house wastewaters. Environ. Technol., 13: 925-936.
2. Foo, K.Y. and B.H. Hameed, 2010. Insights into the modeling of adsorption isotherm systems. Chem. Eng. J., 156: 2-10.
3. Nandi, B.K. and S. Patel, 2017. Effects of operational parameters on the removal of brilliant green dye from aqueous solutions by electrocoagulation. Arabian J. Chem., 10: S2961-S2968.
4. Lakshmi, U.R., V.C. Srivastave, D.I. Mall and D.H. Lataye, 2009. Rice husk ash as an effective adsorbent: Evaluation of adsorptive characteristics for Indigo Carmine dye. J. Environ. Manage., 90: 710-720.
5. El Qada, E.N., S.J. Allen and G.M. Walker, 2008. Adsorption of basic dyes from aqueous solution onto activated carbons. Chem. Eng. J., 135: 174-184.
6. Lin, S.H. and C.F. Peng, 1994. Treatment of textile wastewater by electrochemical method. Water Res., 28: 277-282.
7. Ahmad, A.L., L.S. Tan and S.R.A. Shukor, 2008. Dimethoate and atrazine retention from aqueous solution by nanofiltration membranes. J. Hazard. Mater., 151: 71-77.
8. Jana, S., M.K. Purkait and K. Mohanty, 2010. Removal of crystal violet by advanced oxidation and microfiltration. Applied Clay Sci., 50: 337-341.
9. Gurses, A., C. Dogar, M. Yalcin, M. Acikyildiz, R. Bayrak and S. Karaca, 2006. The adsorption kinetics of the cationic dye, methylene blue, onto clay. J. Hazard. Mater., B131: 217-228.
10. Mahalakshmi, M., B. Arabindoo, M. Palanichamy and V. Murugesan, 2007. Photocatalytic degradation of carbofuran using semiconductor oxides. J. Hazard. Mater., 143: 240-245.
11. Klimiuk, E., U. Filipkowska and B. Libecki, 1999. Coagulation of wastewater containing reactive dyes with the use of polyaluminium chloride (PAC). Polish J. Environ. Stud., 8: 81-88.
12. Purkait, M.K., S. DasGupta and S. De, 2004. Removal of dye from wastewater using micellar-enhanced ultrafiltration and recovery of surfactant. Sep. Purif. Technol., 37: 81-92.
13. Martin, M.M.B., J.A.S. Perez, J.L.G. Sanchez, L.M. de Oca, J.L.C. Lopez, I. Oller and S.M. Rodriguez, 2008. Degradation of alachlor and pyrimethanil by combined photo-Fenton and biological oxidation. J. Hazard. Mater., 155: 342-349.
14. Maldonado, M.I., S. Malato, L.A. Perez-Estrada, W. Gernjak, I. Oller, X. Domenech and J. Peral, 2006. Partial degradation of five pesticides and an industrial pollutant by ozonation in a pilot-plant scale reactor. J. Hazard. Mater., 138: 364-369.
15. Abd El-Rahim, W.M., O.A.M. El-Ardy and F.H.A. Mohammad, 2009. The effect of pH on bioremediation potential for the removal of direct violet textile dye by *Aspergillus niger*. Desalination, 249: 1206-1211.
16. Murthy, H.M.R. and H.K. Manonmani, 2007. Aerobic degradation of technical hexachlorocyclohexane by a defined microbial consortium. J. Hazard. Mater., 149: 18-25.
17. Lodha, S., A. Jain and P.B. Punjabi, 2011. A novel route for waste water treatment: Photocatalytic degradation of rhodamine B. Arabian J. Chem., 4: 383-387.
18. Nandi, B.K., A. Goswami and M.K. Purkait, 2009. Adsorption characteristics of brilliant green dye on kaolin. J. Hazard. Mater., 161: 387-395.
19. Can, O.T., M. Kobya, E. Demirbas and M. Bayramoglu, 2006. Treatment of the textile wastewater by combined electrocoagulation. Chemosphere, 62: 181-187.
20. Mohan, N., N. Balasubramanian and C.A. Basha, 2007. Electrochemical oxidation of textile wastewater and its reuse. J. Hazard. Mater., 147: 644-651.
21. Basha, C.A., N.S. Bhadrinarayana, N. Anantharaman and K.M.M.S. Begum, 2008. Heavy metal removal from copper smelting effluent using electrochemical cylindrical flow reactor. J. Hazard. Mater., 152: 71-78.
22. Daneshvar, N., H.A. Sorkhabi and M.B. Kasiri, 2004. Decolorization of dye solution containing Acid Red 14 by electrocoagulation with a comparative investigation of different electrode connections. J. Hazard. Mater., 112: 55-62.
23. Bayramoglu, M., M. Kobya, O.T. Can and M. Sozbir, 2004. Operating cost analysis of electrocoagulation of textile dye wastewater. Sep. Purif. Technol., 37: 117-125.
24. Liang, Z., Y. Wang, Y. Zhou and H. Liu, 2009. Coagulation removal of melanoidins from biologically treated molasses wastewater using ferric chloride. Chem. Eng. J., 152: 88-94.
25. Meghea, A., H.H. Rehner, I. Peleanu and R. Mihalache, 1998. Test-fitting on adsorption isotherms of organic pollutants from waste waters on activated carbon. J. Radioanal. Nucl. Chem., 229: 105-110.
26. Panahi, R., E. Vasheghani-Farahani and S.A. Shojosadati, 2008. Determination of adsorption isotherm for L-Lysine imprinted Polymer. Iran. J. Chem. Eng., 5: 49-55.
27. Nouri, L., I. Ghodbane, O. Hamdaoui and M. Chiha, 2007. Batch sorption dynamics and equilibrium for the removal of cadmium ions from aqueous phase using wheat bran. J. Hazard. Mater., 149: 115-125.
28. Gottipati, R. and S. Mishra, 2010. Application of biowaste (waste generated in biodiesel plant) as an adsorbent for the removal of hazardous bye-methylene blue-from aqueous phase. Braz. J. Chem. Eng., 27: 357-367.
29. Bulut, Y. and H. Aydin, 2006. A kinetics and thermodynamics study of methylene blue adsorption on wheat shells. Desalination, 194: 259-267.
30. Akazdam, S., M. Chafi, W. Yassine, L. Sebbahi, B. Gourich and N. Barka, 2017. Decolourization of cationic and anionic dyes from aqueous solution by adsorption on NaOH treated eggshells: Batch and fixed bed column study using response surface methodology. J. Mater. Environ. Sci., 8: 784-800.

31. Zafar, S.I., M. Bisma, A. Saeed and M. Iqbal, 2008. FTIR spectrophotometry, kinetics and adsorption isotherms modelling and SEM-EDX analysis for describing mechanism of biosorption of the cationic basic dye Methylene blue by a new biosorbent (Sawdust of Silver Fir, Abies Pindrow). Fresen. Environ. Bull., 17: 2109-2121.
32. Amin, M.T., A.A. Alazba and M. Shafiq, 2015. Adsorptive removal of reactive black 5 from wastewater using bentonite clay: Isotherms, kinetics and thermodynamics. Sustainability, 7: 15302-15318.
33. Zhu, Y., D. Wang, X. Zhang and H. Qin, 2009. Adsorption removal of methylene blue from aqueous solution by using bamboo charcoal. Fresen. Environ. Bull., 18: 369-376.
34. Ponnusami, V., S. Vikram and S.N. Srivastava, 2008. Guava (*Psidium guajava*) leaf powder: Novel adsorbent for removal of methylene blue from aqueous solutions. J. Hazard. Mater., 152: 276-286.
35. Ahmad, M.A. and R. Alrozi, 2011. Removal of malachite green dye from aqueous solution using rambutan peel-based activated carbon: Equilibrium, kinetic and thermodynamic studies. Chem. Eng. J., 171: 510-516.
36. El-Khaiary, M.I., 2008. Least-squares regression of adsorption equilibrium data: Comparing the options. J. Hazard. Mater., 158: 73-87.
37. Thompson, G., J. Swain, M. Kay and C.F. Forster, 2001. The treatment of pulp and paper mill effluent: A review. Bioresour. Technol., 77: 275-286.
38. Srivastava, V.C., M.M. Swamy, I.D. Mall, B. Prasad and I.M. Mishra, 2006. Adsorptive removal of phenol by bagasse fly ash and activated carbon: Equilibrium, kinetics and thermodynamics. Colloids Surf. A: Physicochem. Eng. Aspects, 272: 89-104.
39. Edokpayi, O., O. Osemwenkhae, B.V. Ayodele, J. Ossai, S.A. Fadilat and S.E. Ogbeide, 2018. Batch adsorption study of methylene blue in aqueous solution using activated carbons from rice husk and coconut shell. J. Applied Sci. Environ. Manage., 22: 631-635.
40. Kumar, K.V. and S. Sivanesan, 2006. Pseudo second order kinetics and pseudo isotherms for malachite green onto activated carbon: Comparison of linear and non-linear regression methods. J. Hazard. Mater., 136: 721-726.
41. Kumar, K.V., 2007. Optimum sorption isotherm by linear and non-linear methods for malachite green onto lemon peel. Dyes Pigm., 74: 595-597.
42. Piccin, J.S., G.L. Dotto and L.A.A. Pinto, 2011. Adsorption isotherms and thermochemical data of FD&C Red n°40 binding by chitosan. Braz. J. Chem. Eng., 28: 295-304.
43. Langmuir, I., 1918. The adsorption of gases on plane surfaces of glass, mica and platinum. J. Am. Chem. Soc., 40: 1361-1403.
44. Temkin, M.J. and V. Pyzhev, 1940. Kinetics of ammonia synthesis on promoted iron catalysts. Acta Physicochim. URSS, 12: 217-222.
45. Dubinin, M.M., 1960. The potential theory of adsorption of gases and vapors for adsorbents with energetically nonuniform surfaces. Chem. Rev., 60: 235-241.
46. Hobson, J.P., 1969. Physical adsorption isotherms extending from ultrahigh vacuum to vapor pressure. J. Phys. Chem., 73: 2720-2727.
47. Almeida, C.A.P., N.A. Debacher, A.J. Downs, L. Cottet and C.A.D. Mello, 2009. Removal of methylene blue from colored effluents by adsorption on montmorillonite clay. J. Colloid Interface Sci., 332: 46-53.
48. Tahir, H., U. Hammed, M. Sultan and Q. Jahanzeb, 2010. Batch adsorption technique for the removal of malachite green and fast green dyes by using montmorillonite clay as adsorbent. Afr. J. Biotechnol., 9: 8206-8214.
49. Redlich, O. and D.L. Peterson, 1959. A useful adsorption isotherm. J. Phys. Chem., 63: 1024-1024.
50. Sips, R., 1948. On the structure of a catalyst surface. J. Chem. Phys., 16: 490-495.
51. Toth, J., 1971. State equation of the solid-gas interface layers. Acta Chim. Hung., 69: 311-328.
52. Ho, Y.S. and A.E. Ofomaja, 2006. Pseudo-second-order model for lead ion sorption from aqueous solutions onto palm kernel fiber. J. Hazard. Mater., 129: 137-142.
53. Boulinguiez, B., P. Le Cloirec and D. Wolbert, 2008. Revisiting the determination of langmuir parameters-application to tetrahydrothiophene adsorption onto activated carbon. Langmuir, 24: 6420-6424.
54. Subramanyam, B. and A. Das, 2014. Linearised and non-linearised isotherm models optimization analysis by error functions and staqatistical means. J. Environ. Health Sci. Eng., Vol. 12. 10.1186/2052-336X-12-92.
55. Vijayaraghavan, K., T.V.N. Padmesh, K. Palanivelu and M. Velan, 2006. Biosorption of nickel(II) ions onto *Sargassum wightii*: Application of two-parameter and three-parameter isotherm models. J. Hazard. Mater., 133: 304-308.
56. Marquardt, D.W., 1963. An Algorithm for least-squares estimation of nonlinear parameters. J. Soc. Ind. Applied Math., 11: 431-441.
57. Wang, L., J. Zhang, R. Zhao, Y. Li, C. Li and C. Zhang, 2010. Adsorption of Pb(II) on activated carbon prepared from *Polygonum orientale* Linn.: Kinetics, isotherms, pH and ionic strength studies. Bioresour. Technol., 101: 5808-5814.
58. Ng, J.C.Y., W.H. Cheung and G. McKay, 2002. Equilibrium studies of the sorption of Cu(II) ions onto chitosan. J. Colloid Interface Sci., 255: 64-74.
59. Ng, J.C.Y., W.H. Cheung and G. McKay, 2003. Equilibrium studies for the sorption of lead from effluents using chitosan. Chemosphere, 52: 1021-1030.
60. Kooh, M.R.R., M.K. Dahri and L.B. Lim, 2016. The removal of rhodamine B dye from aqueous solution using *Casuarina equisetifolia* needles as adsorbent. Cogent Environ. Sci., Vol. 2. 10.1080/23311843.2016.1140553.

61. Hamzaoui, M., B. Bestani and N. Benderdouche, 2018. The use of linear and nonlinear methods for adsorption isotherm optimization of basic green 4-dye onto sawdust-based activated carbon. J. Mater. Environ. Sci., 9: 1110-1118.
62. Nethaji, S., A. Sivasamy and A.B. Mandal, 2013. Adsorption isotherms, kinetics and mechanism for the adsorption of cationic and anionic dyes onto carbonaceous particles prepared from *Juglans regia* shell biomass. Int. J. Environ. Sci. Technol., 10: 231-242.
63. Dahri, M.K., M.R.R. Kooh and L.B.L. Lim, 2017. Adsorption characteristics of pomelo skin toward toxic Brilliant Green dye. Scientia Bruneiana, 16: 49-56.
64. Ozdemir, A. and C.S. Keskin, 2009. Removal of a binary dye mixture of congo red and malachite green from aqueous solutions using a bentonite adsorbent. Clays Clay Minerals, 57: 695-705.
65. Verma, V.K. and A.K. Mishra, 2010. Kinetic and isotherm modeling of adsorption of dyes onto rice husk carbon. Global NEST J., 12: 190-196.
66. Giles, C.H., D. Smith and A. Huitson, 1974. A general treatment and classification of the solute adsorption isotherm. I. Theoretical. J. Colloid Interf. Sci., 47: 755-765.
67. Tehrani-Bagha, A.R., H. Nikkar, N.M. Mahmoodi, M. Markazi and F.M. Menger, 2011. The sorption of cationic dyes onto kaolin: Kinetic, isotherm and thermodynamic studies. Desalination, 266: 274-280.
68. Subramanyam, B. and A. Das, 2009. Linearized and non-linearized isotherm models comparative study on adsorption of aqueous phenol solution in soil. Int. J. Environ. Sci. Technol., 6: 633-640.
69. Ncibi, M.C., 2008. Applicability of some statistical tools to predict optimum adsorption isotherm after linear and non-linear regression analysis. J. Hazard. Mater., 153: 207-212.
70. Bera, A., T. Kumar, K. Ojha and A. Mandal, 2013. Adsorption of surfactants on sand surface in enhanced oil recovery: Isotherms, kinetics and thermodynamic studies. Applied Surf. Sci., 284: 87-99.
71. Hamdaoui, O. and E. Naffrechoux, 2007. Modeling of adsorption isotherms of phenol and chlorophenols onto granular activated carbon: Part II. Models with more than two parameters. J. Hazard. Mater., 147: 401-411.
72. Ghaffari, H.R., H. Pasalari, A. Tajvar, K. Dindarloo, B. Goudarzi, V. Alipour and A. Ghanbarneajd, 2017. Linear and nonlinear two-parameter adsorption isotherm modeling: A case-study. Int. J. Eng. Sci., 6: 1-11.
73. Ho, Y.S., J.F. Porter and G. McKay, 2002. Equilibrium isotherm studies for the sorption of divalent metal ions onto peat: Copper, nickel and lead single component systems. Water Air Soil Pollut., 141: 1-33.
74. Chen, X., 2015. Modeling of experimental adsorption isotherm data. Information, 6: 14-22.
75. Korotkova, T.G., S.J. Ksandopulo, A.P. Donenko, S.A. Bushumov and A.S. Danilchenko, 2016. Physical properties and chemical composition of the rice husk and dust. Orient. J. Chem., 32: 3213-3219.
76. Kumar, P.S., K. Ramakrishnan, S.D. Kirupha and S. Sivanesan, 2010. Thermodynamic and kinetic studies of cadmium adsorption from aqueous solution onto rice husk. Braz. J. Chem. Eng., 27: 347-355.